Multibeam Bathymetry and CTD-Measurements in two fjord systems in Southeast Greenland

Kristian Kjellerup Kjeldsen[1,2], Wilhelm Weinrebe[3], Jørgen Bendtsen[4,5], Anders Anker Bjørk[1,6], Kurt Henrik Kjær[1]

[1]Centre for GeoGenetics, Natural History Museum, University of Copenhagen, Copenhagen, DK-1350, Denmark
[2]Department of Earth Sciences, University of Ottawa, Ottawa, K1N 6N5, Canada
[3]GEOMAR, Helmholtz-Zentrum für Ozeanforschung, Kiel, 24148, Germany
[4] Arctic Research Centre, Aarhus University, 8000 Aarhus, Denmark.
[5] ClimateLab, Symbion Science Park, Fruebjergvej 3, 2100 Copenhagen O, Denmark.
[6] Department of Earth System Science, University of California, Irvine, CA 92697, USA

Correspondence to: Kristian K. Kjeldsen (kkjeldsen@snm.ku.dk)

Abstract. We present bathymetry and hydrological observations collected in the summer of 2014 from two fjord systems in Southeast Greenland, using *SS Activ* with a multibeam system temporally installed over the side of the ship. Our results provide a detailed bathymetric map of the fjord complex around Skjoldungen Island and the outer part of Timmiarmiut Fjord and show far greater depths compared to the International Bathymetric Chart of the Arctic Ocean. The hydrography collected show different properties in the fjords with the bottom water masses below 240 m in Timmiarmiut Fjord being 1 - 2 °C warmer than in the two fjords around Skjoldungen Island, but data also illustrate the influence of sills on the exchange of deeper water masses within fjords. Moreover, evidence of subglacial discharge in Timmiarmiut Fjord, consistent with satellite observations of ice mélange set into motion, adds to our increasing understanding of the distribution of subglacial meltwater. Data is available through the PANGAEA website https://doi.pangaea.de/10.1594/PANGAEA.860627

1. Introduction

During the past decades the Greenland Ice Sheet has experienced a considerable increase in mass loss associated with speeding up of glaciers and enhanced melting (Khan et al., 2015). An anomalous inflow of subtropical waters driven by atmospheric changes, multidecadal natural ocean variability and a long-term increase in the North Atlantic's upper ocean heat content since the 1950s has, in conjunction with increased meltwater runoff, lead to enhanced submarine melting, which is believed to have triggered the retreat of Greenland's outlet glaciers, partly responsible for the increased ice loss (Straneo and Heimbach, 2013).

In order to better understand oceanic, cryospheric, and geological processes and the interaction between these, a detailed knowledge of the morphology of a given survey area is essential. The International bathymetry chart of the Arctic Ocean (IBCAO) (Jakobsson et al., 2012) provides an overview of the circum-Arctic bathymetry, however, in many of the Greenlandic fjord systems there is little, if any bathymetric data at all, and thereby the resulting gridded bathymetry may be

inadequate. As a result glaciers may appear grounded near or at sea level, whereas in reality the glaciers these are grounded in deeper waters (Andresen et al., 2014; Rignot et al., 2016).

Publication of different datasets are continuously improving the bathymetry around Greenland, e.g.(Arndt et al., 2015; Fenty et al., 2016; Rignot et al., 2015, 2016; Schumann et al., 2012; Williams et al., 2017), even if it is only based on a suite of
5   single-point observations (Andresen et al., 2014) or inversion of gravity data to obtain bathymetry (Porter et al., 2014). Whereas the topography of the onshore area is easily determined from air- and satellite imagery and altimetry (e.g. (Korsgaard et al., 2016; Willis et al., 2015)), the relief of the submarine parts is hidden by the water column and can only be determined with hydro-acoustic methods or with aerial gravimetry. Thus, extensive bathymetric mapping is necessary in order to create a full image of the seafloor morphology.
10   During the summer of 2014 a multibeam echo-sounder was temporarily installed on *SS ACTIV* (Fig.1) and was used to map the seafloor in two fjord systems in Southeast Greenland. Moreover, to obtain knowledge of the water column sound velocity profiles were determined at 11 positions using a CTD-sensor (CTD = conductivity, temperature, depth). The data presented here supplements data acquired during the 2016 field campaign of Ocean Melting Greenland (Fenty et al., 2016), and as a consequence enabled better use of the ship's resources during the 2016 campaign.

15 **1.1 Study Site**

The study area consists of two fjord systems in Southeast Greenland, namely Timmiarmiut Fjord and the fjord systems around Skjoldungen (Fig. 2b). Timmiarmiut Fjord (Fig.2c) is c. 57 km long and reaches the Timmiarmiut Glacier, a marine outlet glacier from the ice sheet. Along the fjord there are different branches and islands of variable sizes, in particular towards the north where the fjord system reaches Heimdal Glacier, another marine outlet glacier from the ice sheet. Both
20   glaciers are fast moving outlets of the Greenland Ice Sheet (Rignot and Mouginot, 2012), with Timmiarmiut glacier being the 15th fastest, but the fjord system also drainages a large number of smaller glaciers and ice caps, both land- and marine-terminating, that are either isolated or in contact with the ice sheet. At the fjord mouth, depths extent down to c. 620 m according to IBCAO (Jakobsson et al., 2012).

The fjord system surrounding Skjoldungen (Fig. 2d) comprise of a northern- and a southern sound, Nørre Skjoldungesund
25   (NSsund; c. 49 km) and Søndre Skjoldungesund (SSsund; c. 52 km), respectively, and a narrow, shallow section (c. 10 km) towards the northwest that links the two sounds. The fjord system drains both local- and ice sheet glaciers and ice caps, with the vast majority being land-terminating, while the large ice sheet based Thrym Glacier enters the fjord directly in the very northwestern part of the fjord system at the head of NSsund. Around Skjoldungen the official nautical chart supplied by Danish Geodata Agency comprise of low density point depth measurements ranging between 179m and 548 m in NSund and
30   between 46 m and 702 m in SSund, while for both NSsund and SSsund IBCAO suggests depths down to c. 20 m. The Fjord system around Skjoldungen Island is annually visited by cruise ships, adding to the importance of mapping of the fjords.

Outside the fjord systems oceanographic conditions are dominated by the East Greenland Coastal Current (EGCC) above the shelf and the East Greenland Current (EGC) located at the shelf break (Sutherland and Pickart, 2008). These drive Polar Surface Water, originating from the Arctic Ocean, and Atlantic Water, originating from the Irminger Sea.

2 Data and Methods

The data sets in this study were collected during July 2014 and comprise of a multibeam data set and 11 CTD profiles. Below follows a description of the system, sensors and components, and the deployment. Figure 3 shows the deployment of the system on-board *ACTIV*. The software used for data acquisition was ELAC Nautik Hydrostar 3.5.3, while post-processing was accomplished using the software packages ELAC Nautik HDPpost and CARIS HIPS as well as the open source software packages MB-System (Caress and Chayes, 1996) and GMT (Wessel and Smith, 1991).

2.1 Seabeam 1050

Multibeam systems are echo-sounder which map the seafloor along a wide swath beneath the vessel. Due to their complexity such systems are generally permanently installed in the hull of survey vessels. On-board *ACTIV* we temporarily installed a portable ELAC Nautik *Seabeam 1050* multibeam system, provided by GEOMAR Helmholtz-Centre for Ocean Research Kiel.

The Seabeam 1050 multibeam echo-sounder collects bathymetry data with beams as narrow as 1.5° by 1.5° and a swath width of up to 153°. The 50 kHz signal achieves a depth range of more than 2,000 m. Different to other multibeam systems, which transmit a full swath of acoustic energy and use directed reception (*beam forming*), the Seabeam 1050 applies beam forming at transmission and reception, thus achieving a very high side lobe suppression of 36 dB with very low error-rates. The disadvantage of this technique is a slightly lower ping rate. The system is completely stabilized for roll of the ship if an adequate motion sensor is installed. The Seabeam 1050 employs two transducer arrays, port and starboard, both capable of transmitting and receiving. Their acoustic planes are tilted 38° to the vertical. The arrays are normally installed fixed to the ship's hull, but on *ACTIV* they were mounted using a steel pole over the side of the vessel. An overview of the technical specifications of the Seabeam 1050 is provided in Table 1.

2.2 Navigation-, Heading- and Motion sensor F180R

The F180R inertial attitude and positioning system from CodaOctopus is an instrument designed to make precise measurements of the vessel attitude (including heading), dynamics and geographical position for use in any marine hydrographic survey application. It is a multi-sensor system consisting of an inertial measurement unit (IMU), built up of three solid-state gyros and three inertial-grade accelerometers, and two survey grade GPS receivers. The IMU of the F180R is built into a separate waterproof pod in order to allow the IMU to be located close to the transducer heads. The F180R

integrates the information provided by the attitude and position sensors and takes advantage of their complimentary attributes to yield a position and attitude solution more stable than either system operating in isolation. The performance specifications of the F180R system are provided in Table 2.

The F180R system performance depends on a variety of external factors, e.g. poor GPS satellite constellation, multipaths of the GPS signals that will cause errors and reduced accuracy of attitude and heading determinations.

2.3 CTD-sensor Sea&Sun CTD48M

The CTD48M (Sea & Sun Marine Tech) memory probe is a small (1.2 kg) microprocessor controlled multi-parameter titanium (except screws) probe for precise marine measurements. The accuracy of the conductivity and temperature sensor is specified as ±0.003 mS/m and ±0.002 °C, respectively. Considering the instrumental drift we estimate the temperature and salinity error to be about ±0.05 °C and ±0.05, respectively. This is well below the temperature and salinity range in the water column reported below. The CTD48M data acquisition rate was set to record data every 1 dbar during both down- and upcast. CTD-profiles were obtained manually using rope and diving lead. Practical salinity (S_P) was calculated by the Sea & Sun Marine Tech software and potential temperature was calculated from (IOC et al., 2010). Only downcast profiles were considered in the analysis below.

2.4 System installation on-board ACTIV

The two multibeam transducers were mounted to a 6 m pole, which was attached to the hull outboards at port side midships using a clamp and a U-shaped clip (Fig. 3a-b). The transducer head was secured by two Dyneema ropes attached to the vessel (Fig. 3c). During transits and in ice covered areas the entire pole could be hoisted up into a safe position (Fig. 3d). The construction was sufficiently stable and easy to manage throughout the entire cruise; however, the hydrodynamic pressure of the water against the pole during the surveys caused a slight bending of the pole. In addition, a collision with an ice floe on July 22 might also have shifted the transducers slightly out of position. Both events likely had an influence on the accuracy of the multibeam data. The multibeam system, as well as the computer for data acquisition, was installed in the wheelhouse (Fig. 3e).

The IMU of the motion sensor F180R was installed on the deck close to the transducer pole. The two GPS antennas were mounted in a distance of 2.003 m apart on a wooden bar, which was temporarily installed on top of the wheelhouse. The motion sensor was set up to determine the motion of the vessel at the positions of the multibeam transducers (remote lever arm calculation). The reference point for the multibeam depth measurements was defined to be a point exactly above the centre point of the transducers at water level.

2.5 Post-setup calibration and limitations

Once the temporary installation was completed several components of the system had to be calibrated. The motion sensor F180R runs a self-calibration scheme, which requires considerable movement of the vessel and continuous good GPS signal.

Initially, the self-calibration failed, however, after re-mounting the GPS-antennas at a position close-by the stern of the vessel to reduce multipath of the GPS signals caused by masts and rig, a new self-calibration procedure of the F180R was performed. At this position a stable operation of the motion sensor was achieved, however, the accuracy of attitude and heading determinations missed the attainable specification (c.f. Table 2).

Moreover, the multibeam system requires a calibration to determine the angular offsets of the transducers from the horizontal (roll offset) and the vertical (pitch offset) axis, respectively. To perform a roll-calibration, a profile of multibeam data over an essentially flat seafloor is recorded on the same line in both directions. When both lines are processed separately, a potential roll offset will lead to different inclinations of the seafloor in the recorded data and the angular offset can be determined. To determine a possible pitch offset, a structure on the seafloor is mapped on two lines in opposite directions along the same profile. A possible pitch offset leads to different positions of the structure in separately processed lines. As no information on the seafloor depth was available beforehand, the calibrations had to be run over "unknown" seafloor. It turned out that the area was not well suited for a roll calibration; however, an estimate of the roll offset of 0.6° could be determined from the recordings and were used during the following days. A significant vertical offset of the transducers had not been detected so the pitch bias was set to 0°.

3 Results and discussions

3.1 Multibeam surveys

The multibeam system was installed on-board *ACTIV* on July 15, 2014, when the vessel anchored in the fjord south of the old Timmiarmiut weather station. Multibeam surveys were carried whenever weather and ice conditions as well as the scientific program allowed until the system was dismounted on the evening of July 28, 2014. The total track length of the multibeam surveys was 402 km recorded in 54.86 hours and based on a total of 74,502 pings.

3.1.1 Timmiarmiut area survey

Multibeam surveys in the Timmiarmiut area were carried out on July 16, 17, 18, and 28. July 16 and 17 were used to calibrate the setup and re-configure the original installation. The survey in the Timmiarmiut Fjord area was continued on July 18 and July 28, however, due to numerous ice floes and icebergs only a part of the fjord was mapped (Fig. 4a). The survey shows that at least the outer part of the fjord consists of depths down to c. 1060 m. A blow-up of the mouth of Timmiarmiut Fjord is provided in Figure 5a. At a cross-section at the fjord mouth the deepest part is found along a c. 2 km wide section in the middle where depths range between 740 and 830 m. North of this mid-section depths increase from c. 780 m to c. 95 m over a distance of c. 1.2 km, whilst south of the mid-section depths increase from 780 m to c. 190 m over a c. 2 km stretch, intervened by a 1 km wide and c. 150 m deep trough that extends down to c. 550 m, which further up fjord increases to c. 450 m. The general configuration of a wide deep cross-section with great depths is characteristic for the outer

well surveyed area, which covers c. 15 km from the mouth and up fjord, but it also seems to reassemble the branch towards the north covered by the red line in Figure 4a despite the poorer multibeam coverage. In order to compare to existing data we extract data from the deepest part of the fjord in the along fjord direction (Fig. 4b, black and red lines), which range between c. 800 and 880 m. Figure 4b show data extracted from IBCAO (Jakobsson et al., 2012) along the three center lines, green,

5 red, and black. Our new data shows that along the surveyed center line data the fjord is on average 325 m deeper were data overlap. Note that along the inner part of the fjord (green line) IBCAO contains values above sea level. Following our data collection in 2014, the Oceans Melting Greenland (OMG) mission (Fenty et al., 2016) acquired data in Timmiarmiut Fjord during their 2016 cruise. With the knowledge of our data, OMG were able to collected data to supplement our mapping effort, and thus saving time and enabling better use of the ship's resources.

10 **3.1.2 Skjoldungen Fjord survey**

In the Skjoldungen Fjord complex around Skjoldungen Island the multibeam system was deployed on July 20, 21, 22, 23, 24 and 26. Nearly the entire Fjord area was surveyed, leaving only a small gap of 5 km in the innermost part of the fjord system and small unmapped stripes close to the shorelines. Whenever possible, the fjord was mapped along three lines: one in the centre, one closer to the northern and one closer to the southern shore. The innermost stretch of the fjord area could not be

15 mapped as the slopes of the surrounding mountains were too steep for the motion sensor to maintain its GPS-connection, and thus the multibeam system lacked navigation, heading and motion information. Besides this small gap, a comprehensive map of the entire Skjoldungen Fjord area can now be presented for the first time (Fig. 4c). Figure 4d shows the bathymetry from our new data and IBCAO extracted at the center lines of the two fjords. Note that the IBCAO data set here contains values above sea level.

20 Generally, the fjord width around Skjoldungen Island varies between 1.1 km and 3.1 km, except for a narrow stretch along SSsund, where the fjord width narrows down to c. 600 m, and along a small stretch along the innermost unmapped part, where the width narrows down to c. 580 m.

The bathymetry map of the Skjoldungen Fjord complex displays water depths up to 800 m (Fig. 4c and d). The deepest part is a stretch of about 10 km in SSsund. Generally, the southern fjord features an outer deep part showing water depths

25 between 500 m and 800 m and a shallow inner part with depths never reaching more than 300 m. In between the outer and inner parts along the narrowing of the fjord, there is a prominent sill with depths only extending down to c. 77 m (green arrow, Fig. 4c-d and a blow-up is provided in Fig. 5b). Interestingly, in the field we observed multiple lateral moraines on land on either valley side dipping concave down towards the sill or close by. On Digital Elevation Models and orthophotos from 1981 (Korsgaard et al., 2016) the lateral moraines are detectable, however the actual structure and extend of the

30 moraines is difficult to assess. The age of these moraines has yet to be determined, but their presence suggest that the sill and bedrock outcrop that forces the narrowing of the fjord, acted as a pinning point of the receding glacier during deglaciation of the fjord.

The bathymetry of the NSsund is remarkably different from the bathymetry of the SSsund. NSsund shows a more gradual increase of water depths from 85 m in the very inner part to c. 590 m at the entrance with a few undulations along the fjord and local high of c. 210 m (red arrow, Fig. 4c-d). However, in the vicinity of this local high point, only part of the area was surveyed and thereby a deeper path in the non-surveyed area of the bend could be possible, thus making our data a minimum

5   estimate of the limiting depth of NSsund. At the fjord entrance leading to Thrym Glacier the water depth in NSsund is c. 340 m (blue bar, Fig. 4c-d).

In the non-surveyed area in the northwestern part of the fjord complex where SSsund and NSsund are connected, water depth is likely limited and perhaps the deepest points in either end reflected the maximum depth. However, a moraine complex, making the Little Ice Age maximum extent of a local glacier originating from Skjoldungen Island, extends halfway into the

10   fjord and likely cause the fjord to be fairly shallow.

Around Skjoldungen Island IBCAO (Jakobsson et al., 2012) displays only a limited number of grid cells with negative values. Along the longitudinal profile data overlapping data from this study IBCAO data range between 15 m and 390 m with an increase in depth out on the shelf (Fig. 4d). The above sea level values in the IBCAO dataset, both around Skjoldungen Island and in Timmiarmiut Fjord, is in part due to the 500 x 500 m resolution of the data not fully being capable

15   of resolving narrow fjords, but more likely data not being available or incorporated into the final dataset.

Offshore the Skjoldungen fjord complex we further surveyed a small shoal (magenta arrow, Fig. 4b). At the position 63°07.5'N, 41°11.0'W a very shallow area was mapped, the seafloor at this position showed water depths as shallow as 13 m. Surveying along two additional profiles, the extent of this feature could be outlined; unfortunately right on the shallowest position an iceberg was stranded, so this spot could not be mapped. This submarine feature has dimensions of c. 800 m by

20   400 m and a height of c. 200 m.

3.1.3 Constraints and limitations of the multibeam survey

The part of the area mapped during the *SS ACTIV* cruise in 2014 has never been surveyed before using a multibeam system, and furthermore, for great parts of the region no sounding information was available at all. The conditions for multibeam surveys in this area, and particularly on this cruise, were difficult, and of course this has affected the quality of the data.

25   Multibeam transducers are usually permanently installed in the hull of a vessel. For precise measurements of the water depth the transducers have to be mounted such that their three axes are aligned horizontally, vertically, and in the direction of the centre line of the vessel. Minimal deviations are determined by a calibration scheme following the installation. On *SS ACTIV* the transducers were installed temporarily at the lower end of a pole of 6 m length, which was then mounted over the side of the vessel. Of course this cannot be as stable as an installation flush in the hull. The pole is prone to vibrations, and in

30   addition the hydrostatic pressure on the pole while deployed in the water and when moving, led to slight bending of the pole. Also floating ice in the water collided with the pole, moving it slightly out of position. A proper survey would have required at least a roll calibration each time the pole was deployed into the water; however, the area was not well suited for a roll

calibration, which should be run over absolutely planar seafloor. As a makeshift, transit lines run in opposite directions roughly along the same line were used throughout the survey to check and correct the roll bias values.

The motion sensor F180R, used during the survey, needs continuously good connection to GPS satellites, and this was very difficult to maintain inside the fjords. Thus, the achieved heading accuracies and motion information often exceeded the intended specifications, leading to a decreased quality of the multibeam data. Other sources of errors in the data are missing tidal information, frequent changes in the water sound velocity due to the influence of melt water as well as abrupt course changes of the vessel due to ice floes.

However, in spite of the aforementioned problems the results of the multibeam surveys clearly demonstrate that it is actually possible using a ship such as the *SS ACTIV* and a temporary installation, to achieve bathymetric maps of satisfactory quality, even under difficult conditions in remote areas.

3.2 CTD-measurements

During the *SS ACTIV* cruise the CTD was deployed 11 times (Table 3). Locations of the profiles are displayed on Fig. 2c-d. Two of the 11 profiles were obtained in shallow waters while the ship was an anchored and only the top 13-14 m of the water column was sampled. Three CTD profiles were obtained from Timmiarmiut Fjord (TF), four from SSsund and two from NSsund. Note that the vessel drifted during the recording of CTD14-03 causing the water depth to vary.

Figure 6 illustrates the temperature- and salinity profiles and the corresponding temperature-salinity (T-S) plots from the 9 deeper profiles, divided into those from Timmiarmiut Fjord (a and d), SSsund (b and e), and NSsund (c and f), respectively.

In Timmiarmiut Fjord (Fig. 6a and d) three profiles were recorded reaching depths between 285 m and 700 m. The innermost profile was recorded on 18 July, roughly midway between the fjord mouth and Timmiarmiut- and Heimdal glacier, whilst the two other profiles were recorded ten days later on 28 July closer to the fjord mouth. The three profiles show certain similarities but also differences, with the two outermost profiles being almost identical throughout the profiles. For all three profiles the top consists of a pronounced cold layer between c. 120 and 30 m with temperatures less than 0°C and underlying a relatively then, low-saline (S<32) and warm surface layer. However, the transition to the layers below differs as CTD14-01 shows a gradual warming and increasing salinity from c. 110 m to c. 175 m, whilst at the fjord mouth the same conditions are reached already at a depth of c. 125 m. At c. 240 m the three profiles again start to deviate, with the midway profile generally being cooler by more than 1°C at some depths.

Interestingly, the top c. 40 m of the water column at profile CTD14-01 shows a clear difference compared to the two other profiles near the fjord mouth. Here temperatures are cooler and more saline compared to the fjord mouth. This is a strong indication of mixing with subglacial water and, thereby, subglacial discharge from a tidewater outlet glacier in the fjord (Mortensen et al., 2013). Subglacial meltwater discharge causes a buoyant ascending plume near the glacier where meltwater is mixed with high-saline bottom water (Bendtsen et al., 2015) and thereby the salinity in the upper water column may increase significantly (Kjeldsen et al., 2014). Thus, the high salinities observed in the layer between c. 50 - 10 m at station

14-01 can be explained as subglacial water from a tidewater outlet glacier. This is further supported by satellite observation from the period before the CTD profile was measured. MODIS imagery from 10-22 July 2014 (Fig. 7), shows a large pool of ice mélange near the calving front of Heimdal Glacier, north of the CTD-station 14-01, is set into motion and directed away from the terminus by 12 July. By 17 July a large area of the inner fjord is covered by ice reaching midway between Heimdal

5   Glacier and the CTD station. Thus, the high salinities between 50 - 10 m depth can be explained by subglacial water originating from the Heimdal tidewater outlet glacier and the relatively low temperatures in the upper 50 m can be explained by heat loss due to melting of the icebergs.

In SSsund four profiles (Fig. 6b and e) were recorded 21 July and 24 July, two seawards of the sill (Fig4c-d, green arrow),

10   one on the sill, and one landwards of the sill, respectively. The deepest reached 420 m and was recorded mid fjord seawards of the sill, CTD14-02. Generally, the four profiles show the same properties down through the water column, with a fresh warm surface layer overlaying a layer of Polar Water that extends down to 200 m. Further below at greater depth the water column appears homogenous with a constant temperature and salinity, though this is based only on a single profile that reaches 238 m (CTD14-08) and another that reaches 420 m (CTD14-02).

15   Interestingly, below c. 110 m profiles landwards- and seawards of the sill begin to deviate from each other, with CTD14-03 (landwards) being c. 0.6 °C cooler and 0.4 units more fresh. Possibly, this reflects a deeper-lying local water mass occupying the basin between the sill and the northwestern part of the fjord complex, as the inner part connecting SSsund and NSsund is likely shallow due the presence of a moraine complex, thus limiting the exchange of deeper water masses.

20   In NSsund (Fig. 6c and f) two deeper and one shallow profile were recorded. The shallow profile (CTD14-05) is omitted as it reassembles the close-by deeper profile, CTD14-06. The latter is recorded landwards of the sill (Fig. 4c-d, red arrow), whilst CTD14-07 was recorded mid-way between the sill and the fjord mouth. In the upper-most part the profiles look alike with CTD14-06 showing a slightly stronger stratification near 140 m, while at depth the deviation between the two profiles starts to become more obvious. Below c. 185 m CTD14-07 gradually becomes warmer and more saline through to the

25   deepest measurement at 323 m. Contrary; below c. 185 m CTD-1406 remains unchanged with depth. This difference reflects limited water exchange in the deeper parts of the fjord, and thus supports the presence of a sill, in accordance with the recorded bathymetry.

Relatively cold water masses characterize the three fjords in the upper c. 120 m and, except for the presence of subglacial

30   water in the innermost profile in Timmiarmiut Fjord, which has a local origin, the upper water masses share the same temperature and salinity characteristics. The deeper part of the fjords show some differences where the bottom water masses below 240 m in Timmiarmiut Fjord are 1 - 2 °C warmer than in the other two fjords. This indicates a stronger influence from mixing with warmer water masses in Timmiarmiut Fjord.

The regional oceanographic conditions outside the fjord systems are dominated by the East Greenland Coastal Current (EGCC) above the shelf and the East Greenland Current (EGC) located at the shelf break (Sutherland and Pickart, 2008). The shelf is c. 2-300 m deep outside the fjords and c. 40-50 km wide. Upper water masses on the shelf is characterized by Polar Surface Water ($\theta < 0$ °C, $\sigma_\theta < 27$ kg m^{-3}) (Sutherland and Pickart, 2008) originating from the Arctic Ocean and

5   influenced by melted ice and runoff. The Atlantic water is located on the shelf break and originates from the Irminger Sea and from re-circulated water from the North Atlantic Current further east between Iceland and the Faeroe Islands. Bottom water masses inside the fjords are relatively cold and from the Temperature-Salinity diagram (Fig. 8) they are located at the mixing line between Atlantic Water (AW, $4.5 < \theta < 6.5$ °C, $34.8 < S_P < 35.0$) and PSW. Water masses below 120 m are relatively cold and below 4°C, which indicate a limited exchange between the deeper part of the fjords and the warm

10   Atlantic Water mass. However, the relatively warm bottom water masses in Timmiarmiut Fjord compared with the two other fjords further north could indicate a larger influence from warm Atlantic Water here, possibly due to the relatively narrow width of the shelf outside the fjord.

4 Conclusions

In this study we have presented bathymetrical data obtained during a cruise in 2014 using a multibeam system temporarily

15   installed on *SS ACTIV*. The data collected provide new insights into fjords with limited information of the bathymetry, but also supplements subsequent large-scale data collection from the OMG mission. The need for new data is evident when comparing to existing data such as IBCAO or single point-measurements from nautical maps. These new efforts provide better spatial resolution, and importantly, also a better description of depths and the seafloor morphology. For instance comparison to IBCAO shows not only greater depths (Fig. 4b), but also that the 500 m spatial resolution of IBCAO is

20   insufficient to properly distinguish between land and fjord in these narrow fjord settings, and likely the single-point measurements from the nautical charts, for instance around Skjoldungen Island, where not included in IBCAO, leading to considerable discrepancy between that and data from this study. However, with the single major objective of IBCAO being to provide a portrayal of the Arctic Ocean seafloor (Jakobsson et al., 2012), it is understandable that not all fjord complexes are as well resolved as offshore bathymetry based on extensive multibeam mapping. However, large-scale efforts such as the

25   OMG mission measuring bathymetry (Fenty et al., 2016) and the synthetic bathymetry datasets (Williams et al., 2017) are beginning to shed new light on the configurations of fjords around Greenland.

The CTD-measurements collected during the cruise provide information about the properties of the water column in relation to sound velocity and the bathymetrical mapping, but they allow an insight into the distribution of water masses in the different fjord settings. Here we find considerable difference between the water masses located in the three fjord settings,

30   influenced not only by the local bathymetry, such that sills in SSsund and NSsund hinder exchange of deeper warmer water masses that might affect the marine terminating Thrym Glacier at the head of the fjord, but the variability in the influence of Atlantic Water flowing on the shelf outside the fjords, causing deeper water in Timmiarmiut Fjord to be warmer relative to

the fjords around Skjoldungen Island further north. Moreover, high salinities are observed in the layer between c. 50 - 10 m in the inner part of Timmiarmiut Fjord, suggesting release of subglacier meltwater from Heimdal Glacier upfjord of the CTD-station, consistent with satellite imagery that show a large pool of ice mélange set into motion five days prior to our CTD measurements.

5   Observations presented in this study complements large-scale efforts to obtain knowledge about the bathymetry and hydrography in the fjords around Greenland, but they adds to our understanding of how subglacial meltwater is distributed in fjord systems and the impact on fjord circulation (Bendtsen et al., 2015; Kjeldsen et al., 2014), important for understanding how a future warming ocean will affect the stability of marine terminating outlet glaciers.

10 The authors declare that they have no conflict of interest.

Acknowledgement:

We thank GEOMAR Helmholtz-Centre for Ocean Research Kiel for graciously lending us their *Seabeam 1050* multibeam system, Wärtsilä ELAC Nautik for lending us a transducer mounting frame, and Teledyne CARIS for providing the software CARIS HIPS. Moreover, we thank the crew on-board *SS ACTIV* for their help collecting the data during the field campaign.
15 KKK acknowledges support from the Danish Council Research for Independent research (grant no. DFF - 4090-00151). AAB was supported by the Danish Council for Independent Research, grant DFF-610800469 and by the Inge Lehmann Scholarship from the Royal Danish Academy of Science and Letters.

Caress, D.W. & Chayes, D.N.: Improved processing of Hydrosweep DS multibeam data on the R/V Maurice Ewing, Marine
20 Geophysical Researches 18: 631. doi:10.1007/BF00313878, 1996
Wessel, P. and Smith, W. H. F.: Free software helps map and display data, EOS Trans. AGU, 72, 441, 1991

References

Andresen, C. S., Kjeldsen, K. K., Harden, B., Nørgaard-Pedersen, N. and Kjær, K. H.: Outlet glacier dynamics and
25 bathymetry at Upernavik, Geol. Surv. Denmark Greenl. Bull., 31, 79–82, 2014.
Arndt, J. E., Jokat, W., Dorschel, B., Myklebust, R., Dowdeswell, J. A. and Evans, J.: A new bathymetry of the Northeast Greenland continental shelf: Constraints on glacial and other processes, Geochemistry, Geophys. Geosystems, 16(10), 3733–3753, doi:10.1002/2015GC005931, 2015.
Bendtsen, J., Mortensen, J., Lennert, K. and Rysgaard, S.: Heat sources for glacial ice melt in a west Greenland tidewater
30 outlet glacier fjord: The role of subglacial freshwater discharge, Geophys. Res. Lett., 42(August 2013), 4089–4095,

doi:10.1002/2015GL063846, 2015.

Caress, D. W. and Chayes, D. N.: Improved processing of Hydrosweep DS multibeam data on the R/V Maurice Ewing, Mar. Geophys. Res., 18(631), doi:10.1007/BF00313878, 1996.

Fenty, I., Willis, J. K., Khazendar, A., Dinardo, S., Forsberg, R., Fukumori, I., Holland, D., Jakobsson, M., Moller, D., Morison, J., Münchow, A., Rignot, E., Schodlok, M., Thompson, A. F., Tinto, K., Rutherford, M. and Trenholm, N.: Oceans Melting Greenland: Early Results from NASA's Ocean-Ice Mission in Greenland, Oceanography, 29(4), 72–83, doi:https://doi.org/10.5670/oceanog.2016.100, 2016.

IOC, SCOR and IAPSO: The international thermodynamic equation of seawater – 2010: Calculation and use of thermodynamic properties, Intergov. Oceanogr. Comm. Manuals Guid., 56, 1–196, 2010.

Jakobsson, M., Mayer, L., Coakley, B. J., Dowdeswell, J. A., Forbes, S., Fridman, B., Hodnesdal, H., Noormets, R., Pedersen, R., Rebesco, M., Schenke, H. W., Zarayskaya, Y., Accettella, D., Armstrong, A., Anderson, R. M., Bienhoff, P., Camerlenghi, A., Church, I., Edwards, M., Gardner, J. V., Hall, J. K., Hell, B., Hestvik, O., Kristoffersen, Y., Marcussen, C., Mohammad, R., Mosher, D., Nghiem, S. V., Pedrosa, M. T., Travaglini, P. G. and Weatherall, P.: The International Bathymetric Chart of the Arctic Ocean (IBCAO) Version 3.0, Geophys. Res. Lett., 39(12), 1–6, doi:10.1029/2012GL052219, 2012.

Khan, S. A., Aschwanden, A., Bjørk, A. A., Wahr, J., Kjeldsen, K. K. and Kjær, K. H.: Greenland ice sheet mass balance: a review, Reports Prog. Phys., 78, doi:10.1088/0034-4885/78/4/046801, 2015.

Kjeldsen, K. K., Mortensen, J., Bendtsen, J., Petersen, D., Lennert, K. and Rysgaard, S.: Ice-dammed lake drainage cools and raises surface salinities in a tidewater outlet glacier fjord, west Greenland, J. Geophys. Res. Earth Surf., 119, 1310–1321, doi:10.1002/2013JF003034, 2014.

Korsgaard, N. J., Nuth, C., Khan, S. A., Kjeldsen, K. K., Bjørk, A. A., Schomacker, A. and Kjær, K. H.: Digital elevation model and orthophotographs of Greenland based on aerial photographs from 1978–1987, Sci. Data, 3, 160032, doi:10.1038/sdata.2016.32, 2016.

Mortensen, J., Bendtsen, J., Motyka, R. J., Lennert, K., Truffer, M., Fahnestock, M. and Rysgaard, S.: On the seasonal freshwater stratifi cation in the proximity of fast-flowing tidewater outlet glaciers in a sub-Arctic sill fjord, J. Geophys. Res. Ocean., 118, 1382–1395, doi:10.1002/jgrc.20134, 2013.

Porter, D. F., Tinto, K. J., Boghosian, A., Cochran, J. R., Bell, R. E., Manizade, S. S. and Sonntag, J. G.: Bathymetric control of tidewater glacier mass loss in northwest Greenland, Earth Planet. Sci. Lett., 401, 40–46, doi:10.1016/j.epsl.2014.05.058, 2014.

Rignot, E. and Mouginot, J.: Ice flow in Greenland for the International Polar Year 2008–2009, Geophys. Res. Lett., 39(11), L11501, doi:10.1029/2012GL051634, 2012.

Rignot, E., Fenty, I., Xu, Y., Cai, C. and Kemp, C.: Undercutting of marine-terminating glaciers in West Greenland, Geophys. Res. Lett., 42(14), 5909–5917, doi:10.1002/2015GL064236, 2015.

Rignot, E., Fenty, I., Xu, Y., Cai, C., Velicogna, I., Cofaigh, C., Dowdeswell, J. A., Weinrebe, W., Catania, G. and Duncan,

D.: Bathymetry data reveal glaciers vulnerable to ice-ocean interaction in Uummannaq and Vaigat glacial fjords , west Greenland, Geophys. Res. Lett., 2014(Figure 1), 1–8, doi:10.1002/2016GL067832.Received, 2016.

Schumann, K., Völker, D. and Weinrebe, W. R.: Acoustic mapping of the Ilulissat Ice Fjord mouth, West Greenland, Quat. Sci. Rev., 40, 78–88, doi:10.1016/j.quascirev.2012.02.016, 2012.

5   Straneo, F. and Heimbach, P.: North Atlantic warming and the retreat of Greenland's outlet glaciers, Nature, 504(7478), 36–43, doi:10.1038/nature12854, 2013.

Sutherland, D. A. and Pickart, R. S.: Progress in Oceanography The East Greenland Coastal Current : Structure , variability , and forcing, , 78, 58–77, doi:10.1016/j.pocean.2007.09.006, 2008.

Wessel, P. and Smith, W. H. F.: Free software helps map and display data, EOS Trans. AGU, 72(441), 1991.

10   Williams, C. N., Cornford, S. L., Jordan, T. M., Dowdeswell, J. A., Siegert, M. J., Clark, C. D., Swift, D. A., Sole, A., Fenty, I. and Bamber, J. L.: Generating synthetic fjord bathymetry for coastal Greenland, Cryosph., 11, 363–380, doi:10.5194/tc-11-363-2017, 2017.

Willis, M. J., Herried, B. G., Bevis, M. G. and Bell, R. E.: Recharge of a subglacial lake by surface meltwater in northeast Greenland, Nature, 518(7538), 223–227, doi:10.1038/nature14116, 2015.

Figure 1: The three masted wooden schooner *SS ACTIV*.

Figure 2: Map of the locations, with inserts showing the Timmiarmiut Fjord system (c) and the fjord complex around Skjoldungen Island with Nørre Skjoldungesund (NSsund) towards the north and Søndre Skjoldungesund (SSsund) towards the south (d).

Figure 3: Deployment of the multibeam system on-board *ACTIV* using a clamp and a U-shaped clip (a-b). (c) illustrates the system during the surveying mode, while (d) illustrates the system in the safe position used for transits. The multibeam system and computers were in installed in the wheelhouse (e).

Figure 4: Surveyed bathymetry in Timmiarmiut Fjord system (a). The three colored lines follow the deepest part along the fjords and are illustrated in (b), representing the outer well surveyed area (black line), the brach towards the north leading to Halifaxe Glacier at the head, and towards Timmiarmiut Glacier (green line). The surveyed bathymetry around Skjoldungen Island is illustrated in (c), while (d) shows the longitudinal profiles of Søndre Skjoldungesund (black lines) and Nørre Skjoldungesund (red lines). Green-, red-, and magenta arrows in (c) and (d) indicate the prominent sill in SSsund, the local high in NSsund, and the offshore shoal, respectively. For the profiles in both (b) and (d) bathymetry obtained from IBCAO is included.

Figure 5: Blow-up of the mapped bathymetry at the mouth of Timmiarmiut Fjord (a) and around the sill region in SSsund (b). both maps overlay a 1981 orthophoto derived from aerial imagery.

Figure 6: Temperature- and salinity profiles and the corresponding T-S diagrams for Timmiarmiut Fjord (a and d), Søndre Skjoldungesund (b and e), and Nørre Skjoldungesund (c and f), respectively. Approximate sills depths retrieved from the bathymetry data are illustrated in b and c.

Figure 7: MODIS imagery of the inner part of the branch of Timmiarmiut Fjord that leads towards Heimdal at the head. The imagery illustrates he distribution of ice mélange set into motion on 13 July near the calving front of Heimdal glacier due release of subglacial meltwater. During the following days the ice mélange expands and is directed southwards. In our CTD measurements on 18 July from CTD14-01 we detect this as a cooling and as an increase in the salinity of the layer between 10 – 50 m depth.

Figure 8: Potential temperature (θ) - Salinity (S_P) diagram of all profiles from the three fjords. The two stations in Timmiarmiut Fjord near the Heimdal tidewater outlet glacier (CTD14-01 and 14-09) are shown with dashed lines. Temperature-salinity characteristics of two water masses, i.e. Atlantic water (AW) and Polar Surface Water (PSW), are indicated and lines of constant density (σ_θ, kg m^{-3}) are contoured.

Table 1: Overview of the technical specifications of the Seabeam 1050

Table 2: Performance specifications of the F180R system

Table 3: Overview of the 11 CTD-profiles.

Fig. 1
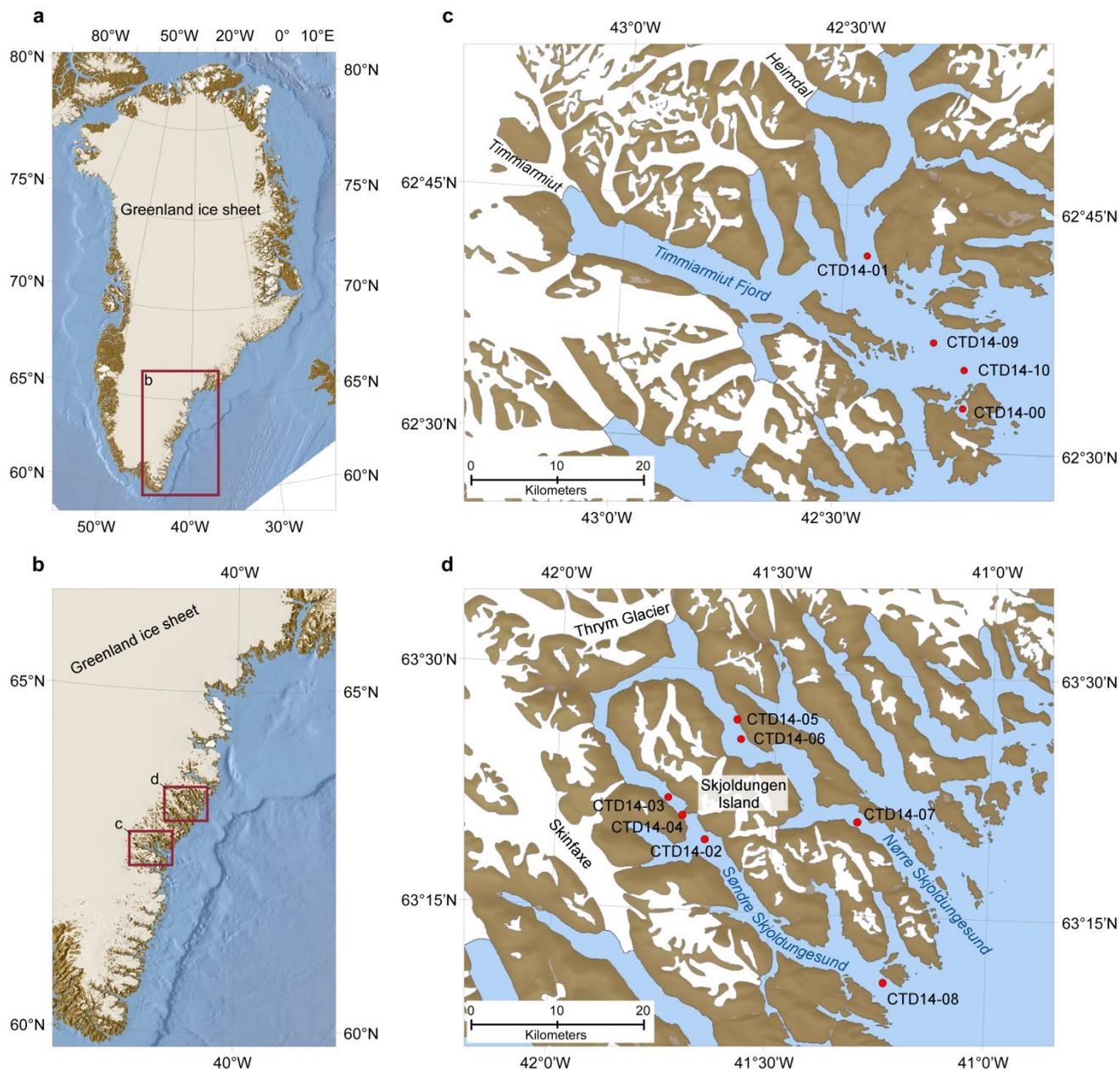
Fig. 2

Fig. 3
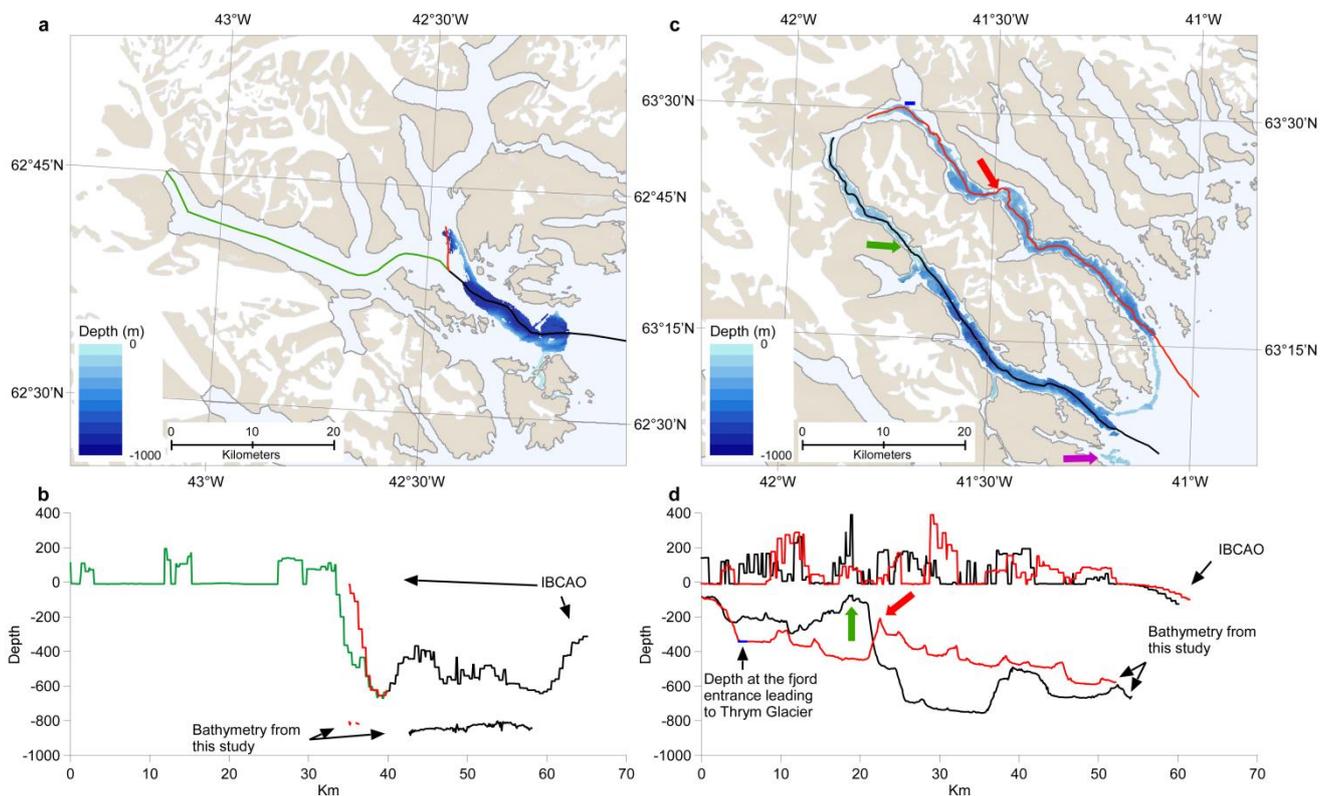
Fig. 4
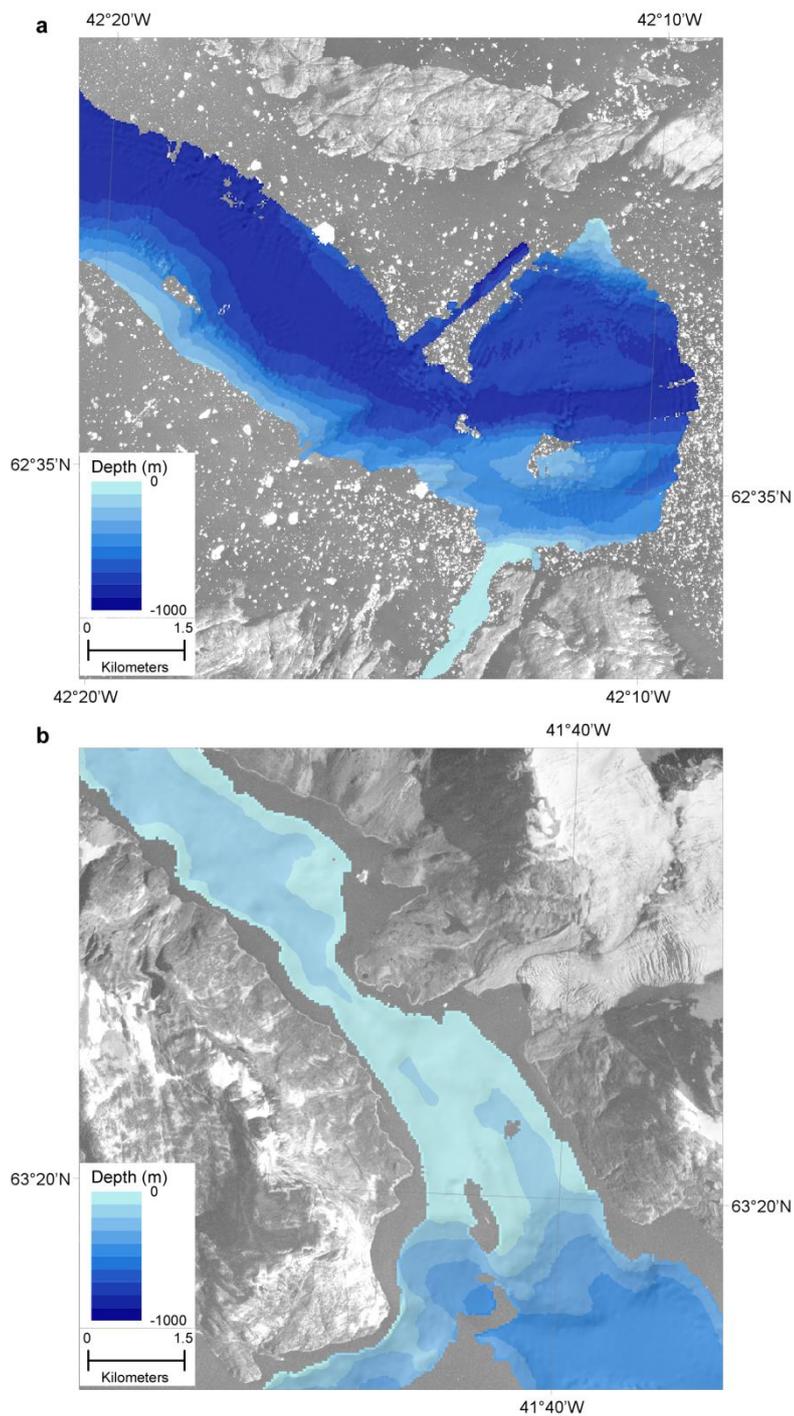
Fig. 5
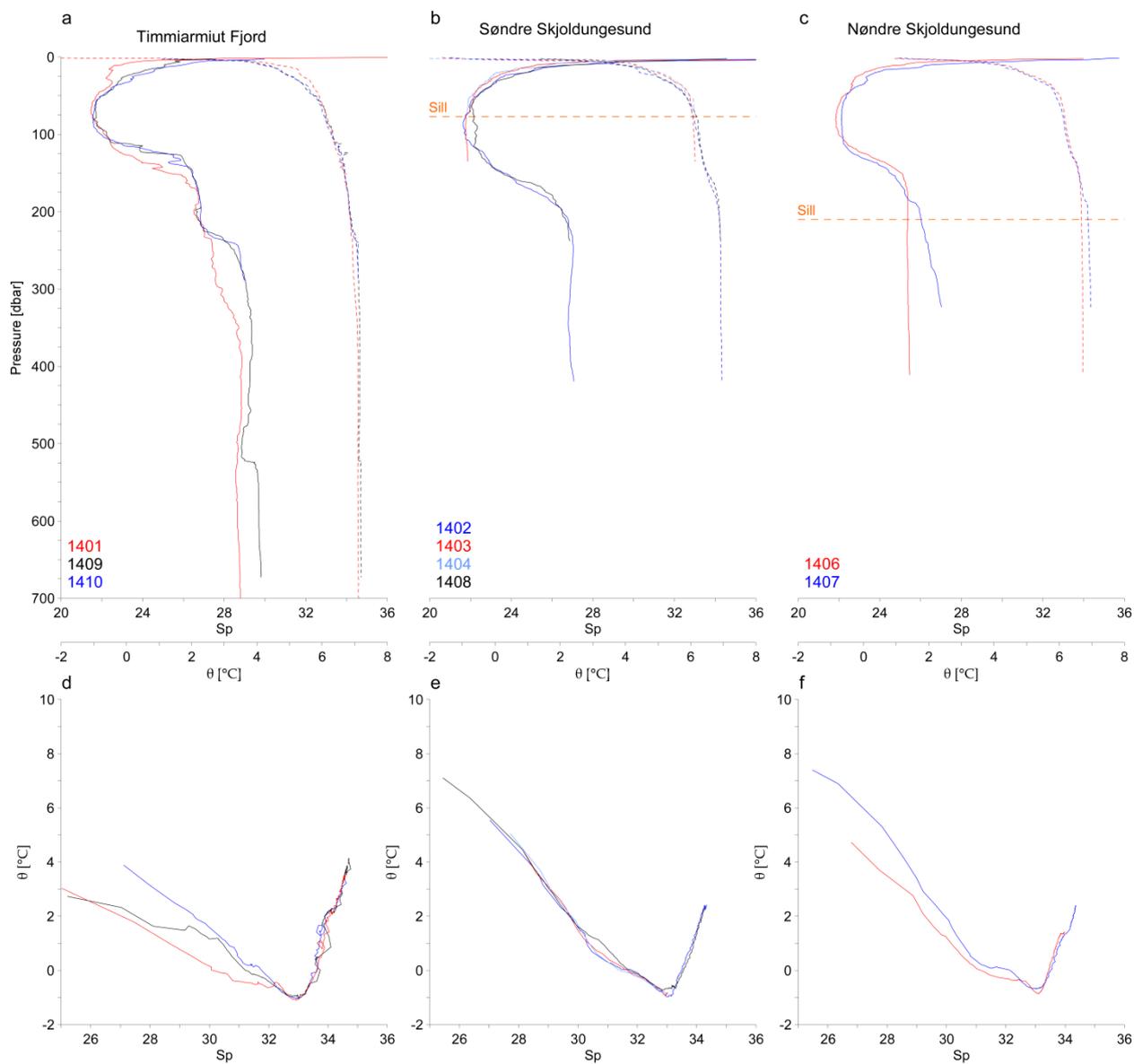
Fig. 6
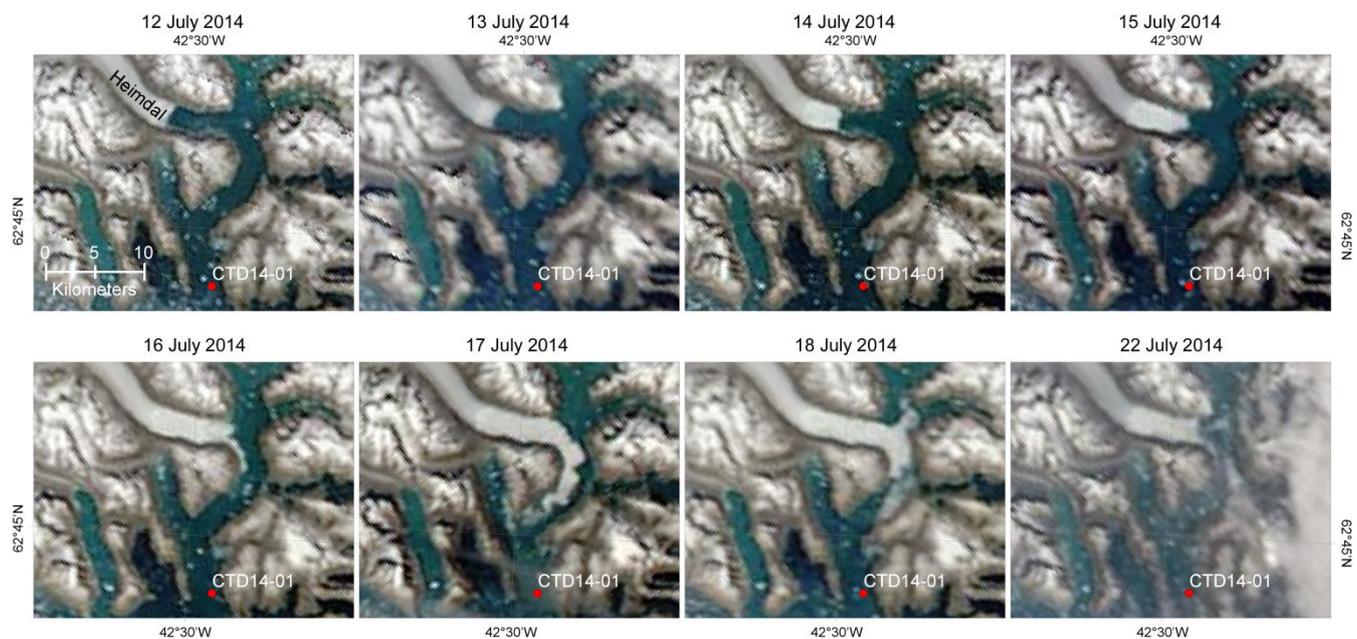
Fig. 7
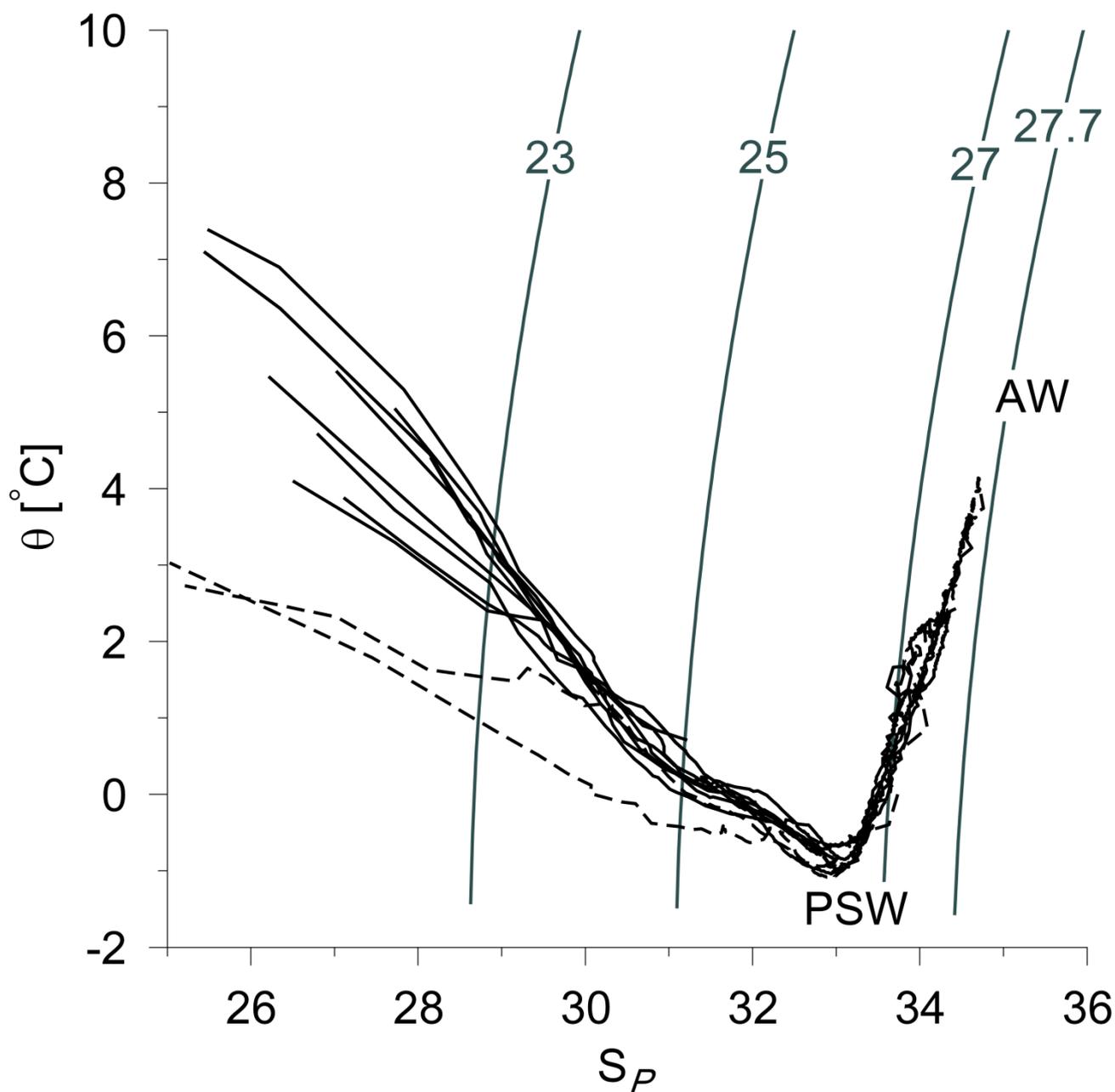
Fig. 8

Table 1

Frequency:	50 kHz
Mmaximum depth:	3,000 m
Beam width:	1.5° by 1.5°
Pulse length:	0.15 ms – 10 ms
Side lobe suppression:	36 dB (transmission and reception)
Maximum swath width:	153°
Maximum number of beams:	126
Beam spacing:	equiangular

Table 2

	According to specification	Achieved during ACTIV survey
Heading accuracy	0.05°	0.46°
Attitude accuracy	0.025°	0.045°
Position accuracy	0.5 m (without DGPS or RTK)	0.49 m
Heave accuracy	5 % of heave amplitude, minimum 5 cm	Not determined

Table 3

Station no.	Date	Fjord system	Latitude (dd.ddddd)	Longitude (dd.ddddd)	Depth of the CTD-profile (m)	Water depth (m)
CTD14-00	16-07-2014	TF	62.52633	-42.18650	14 m	56 m
CTD14-01	18-07-2014	TF	62.69767	-42.44867	707 m	795 m
CTD14-02	21-07-2014	SSsund	63.32350	-41.65467	420 m	454 m
CTD14-03	21-07-2014	SSsund	63.36550	-41.74217	135 m	161 m
CTD14-04	21-07-2014	SSsund	63.34800	-41.70750	75 m	59-90 m*
CTD14-05	22-07-2014	NSsund	63.44933	-41.58950	13 m	13 m
CTD14-06	23-07-2014	NSsund	63.42883	-41.57967	412 m	420 m
CTD14-07	23-07-2014	NSsund	63.34717	-41.30383	323 m	407 m
CTD14-08	24-07-2014	SSsund	63.18167	-41.23200	238 m	238 m
CTD14-09	28-07-2014	TF	62.61100	-42.28933	673 m	826 m
CTD14-10	28-07-2014	TF	62.58450	-42.21767	289 m	400 m